Exploring Multisource Remote Sensing for Assessing and Monitoring the Ecological State of the Mountainous Natural Grasslands in Armenia

Grigor Ayvazyan *, Vahagn Muradyan, Andrey Medvedev, Anahit Khlghatyan, Shushanik Asmaryan

Posted Date: 9 September 2024

doi: 10.20944/preprints202409.0674.v1

Keywords: Multisource remote sensing; mountainous grasslands; UAV data; trend analysis; short-term data sets; vegetation indices; Armenia

Article

Exploring Multisource Remote Sensing for Assessing and Monitoring the Ecological State of the Mountainous Natural Grasslands in Armenia

Grigor Ayvazyan *, Vahagn Muradyan, Andrey Medvedev, Anahit Khlghatyan and Shushanik Asmaryan

Center for Ecological - Noosphere Studies NAS RA, GIS & Remote Sensing Department, Abovyan Str. 68, Yerevan, 0025, Armenia

* Correspondence: Correspondence: grigor.ayvazyan@cens.am; Tel.: (+37498511564)

Abstract: Remote sensing (RS) is a compulsory component in studying and monitoring ecosystems suffering from the disruption of natural balance, productivity, and degradation. Current study attempted to assess the feasibility of multisource RS for assessing and monitoring mountainous natural grasslands in Armenia. Series of the different spatial resolution RS data (Landsat 8, Sentinel 2, Planet Scope, and multispectral UAV data) were used to obtain various vegetation spectral indices: NDVI, NDWI, GNDVI, GLI, EVI, DVI, SAVI, MSAVI, and GSAVI, and the relationship among the indices were assessed via Spearman correlation method, which shows a significant positive correlation for all cases ($p < 0.01$). A comparison of all indices shows a significant high correlation between UAV and the PlanetScope imagery. The comparison of UAV, Sentinel and Landsat data show moderate and low significant correlation ($p < 0.01$) correspondingly. Also, trend analysis was performed to explore their spatial-temporal changes using Mann-Kendall statistical tests (MK, MKKH, MKKY, PW, TFPW), which indicated no significant trend. However, Sen's slope as second estimator shows decreasing trend. Though the best result received for PlanetScope and Sentinel 2, Sentinel-2 data seem to have better alignment making it a reliable tool for an accurate monitoring of small mountainous grasslands in Armenia.

Keywords: Multisource remote sensing; mountainous grasslands; UAV data; trend analysis; short-term data sets; vegetation indices; Armenia

1. Introduction

The Natural grasslands are one of the most important terrestrial ecosystems on earth, covering more than 40% of the land area [1], 70% of the world's agricultural area [2,3] , and providing 30% of the terrestrial biomass [1,4,5]. Grasslands are the main source of livestock feed and solve several human food security problems [6,7], especially in mountainous and crop-poor regions [8–12] . In addition, they also carry out important ecological functions that contribute to the protection of the environment, such as strengthening the soil layer, water and carbon accumulation [1] regulating the circulation of vital elements, water, and nitrogen in nature [7,13,14]. However, nowadays like other environmental ecosystems, natural grasslands are also under the threat of degradation and desertification triggered by many natural and anthropogenic factors [15–19]. All these lead to a significant decrease in productivity and disruption of grassland's ecosystem functions, which creates serious challenges for grassland management and sustainable development[14,20–22]. Therefore, studying and timely and accurate monitoring of changes in the state of grasslands [23–25] (https://www.fao.org/home/en) have a great economic and environmental importance [15]. The mountainous natural grasslands of Armenia have not been spared from this threat, because of the mismanagement of grasslands, overgrazing, and natural factors (erosion, landslide, mudslide), which are even more acute and strongly expressed in the mountainous areas [26].

There are two main methods for the grassland monitoring and study: traditional (field) and remote sensing. Traditional methods include biomass harvesting, eddy covariance tower

 doi:10.20944/preprints202409.0674.v1

measurements, and phenocams [27], and are the most reliable and accurate methods of obtaining information on the condition of grasslands. However, they are time-consuming and labor-intensive, effective at a local scale. However, for large-scale research, they have severe limitations in both spatial and temporal scales[28,29]. In contrast to traditional measurements, satellite and aerial remote sensing has an overall advantage of convenience, efficiency, and cost-effectiveness[1]. Moreover, in the last 20 years, the role of remote sensing technologies in the study and monitoring of grasslands has greatly increased [3] which have the potential for rapid and automated measurements to quantify both structural and biochemical properties of vegetation [25,30,31].

Satellite remote sensing such as LANDSAT, MODIS, SENTINEL, Planet Scope etc, has a primary role in the field of grassland monitoring, and time series analysis. However, they have limitations related to low spatial and temporal resolution [32], and external influences such us cloud cover, shadows, position, and angle of incidence of the solar radiation [1]. It can be complemented mostly by aerial images such as UAV data, likewise validating the result derived from the satellite images [33,34].

The dynamic growth in the use of unmanned aerial vehicles (UAVs) over the last decade, supported by a large number of scientific articles, proves the viability of these devices for monitoring and assessing pasture biomass condition and measuring biophysical parameters [35] and the validation of the satellite data [33]. These devices are flexible, simple and affordable, and most importantly, they allow high spatial and temporal resolution data related to the state of grassland biomass and spatial distribution as needed [20,25,36]. However, these also have several limitations, such as covering relatively small areas, climatic conditions, sometimes financial inaccessibility, etc. Vegetation spectral indices are principal for remote sensing data analysis, in particular for the quantitative and qualitative assessment of vegetation cover, monitoring terrestrial ecosystems, studying vegetation dynamics, and identifying environmental stresses [37,38]. In many studies, vegetation indices based on optical sensors serve as proxies to examine the spatial and temporal patterns of grassland productivity [39–45].

Remote sensing is not actively used enough when studying and monitoring mountain natural grasslands in Armenia. Some studies on inventory of grasslands via visual image processing and mapping were performed within the framework of the CARMAC project funded by World Bank [46]. Afterwards, Tepanosyan et al. developed and evaluated a method of assessing the degradation of grasslands based on spectral analysis of high-resolution Quick Bird imagery [47]. Also, some attempts on multidecadal trend analysis of Armenian grasslands for some study areas in the context of climate change were implemented as well [26,48]. All these studies were performed using single-source data and there is no any approach to compare the data obtained from different remote sensing sources with different spatial and temporal resolutions: satellite sensors and drones, which will make them possible for more detailed and efficient studies of these areas and which is more credible and reliable than single-source data [49–51].

Hence, we aimed to assess the feasibility of multisource remote sensing for (i) productivity analysis of the mountainous natural grasslands in Armenia and (ii) exploring the spatiotemporal changes via trend analysis of the biomass of these grasslands. For this purpose, research questions are set up as follow:

1. A spatial correlation analysis of the space - and UAV-born spectral vegetation indices best reflecting the state of the biomass of grasslands.
2. A trend analysis of grasslands biomass based on remote sensing data.

2. Materials and Methods

2.1. Study Area

The study area is represented by grasslands covering 243 ha of the rural community Nerkin Sasnashen, allocated in the Aragatsotn administrative district (marz) of Armenia. The entire rural community is allocated on the southwestern slope of the Aragats volcanic shield (40°21′23″N 43°59′31″E), extending from north to south [46]. The landscape is represented by mountain-meadow-

 doi:10.20944/preprints202409.0674.v1

steppe (2200-2600m) and subalpine highland (2400-2800m) [46,52]. Atmospheric precipitation in July-August ranges 25–150 mm, and the average air temperature in July ranges 10-22°C. Snow cover lasts from November to May [52].

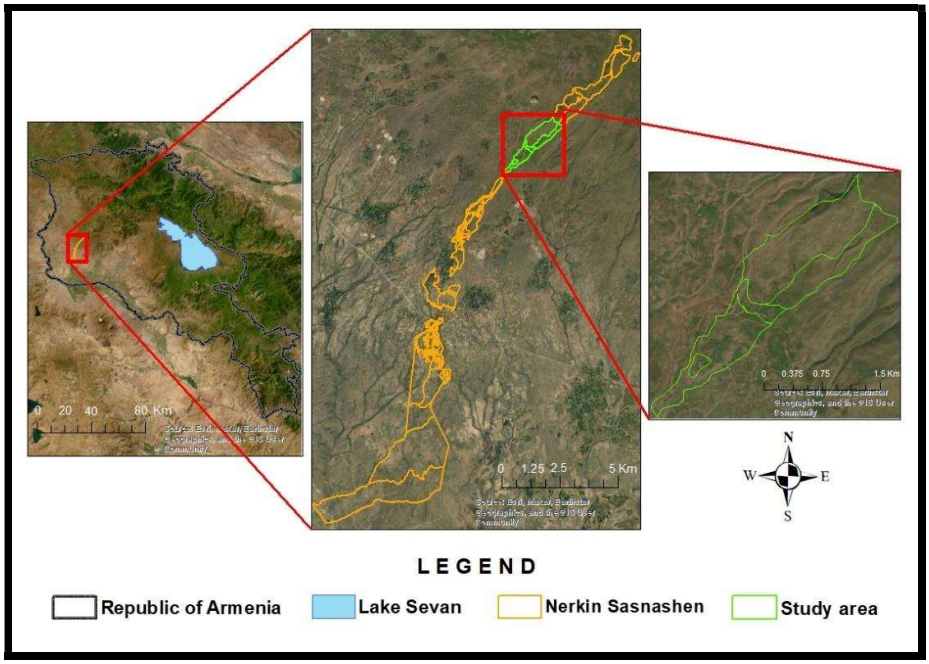

Figure 1. Mountain grasslands of the Nerkin Sasnashen.

2.2. Remote Sensing Data

2.2.1. Satellite Data

Time series of Planet Scope, Sentinel-2, and Landsat 8 satellites (Table…) captured in the period from May to July 2018-2023 were used as input data. We used images from Planet Scope with surface reflectance, obtained from the standard Planet Analytic Product (Radiance), and processed to top-of-atmosphere (TOA) reflectance and then atmospherically corrected to surface reflectance (https://assets.planet.com/docs/Planet_Combined_Imagery_Product_Specs_letter_screen.pdf).

Images from Sentinel-2 Level 2A were atmospherically corrected and with surface reflectance (https://sentinel.esa.int/documents/247904/685211/Sentinel-2_User_Handbook).

Landsat 8 OLI images were Level-2 data products, atmospherically corrected by the Landsat Surface Reflectance Code (LaSRC) method (https://www.usgs.gov/landsat-missions/landsat-collection-2-surface-reflectance).

Both Sentinel-2 and Landsat 8 OLI data were derived from the Google Earth Engine (GEE) platform using a JavaScript application programming interface (API) [26]. The scenes with more than 30% cloud cover were excluded.

For further comparison of the data (Planet Scope, Sentinel-2, Landsat 8, and DJI Phantom 4 Multispectral UAV), satellite images were captured close to 29 June 2023, when a UAV survey was conducted.

Table 1. The Technichal charachteristics of applied RS Space sources.

Satellite	Band Name	Wavelength (nm)	Spatial Resolution (m)	Citation

 doi:10.20944/preprints202409.0674.v1

Planet Scope	Band 1 - Coastal Blue	431 - 452	3	(https://assets.planet.com/docs/Planet_Combined_Imagery_Product_Specs_letter_screen.pdf)
	Band 2 - Blue	465 - 515	3	
	Band 3 - Green	513 - 549	3	
	Band 4 - Green	547 - 583	3	
	Band 5 - Yellow	600 - 620	3	
	Band 6 - Red	650 - 745	3	
	Band 7 - Red Edge	780 - 680	3	
	Band 8 - Near Infrared	845 - 885	3	
Sentinel 2 L2A	Band 1 - Coastal/ Aerosol	433 - 453	60	(https://sentinel.esa.int/documents/247904/685211/Sentinel-2_User_Handbook)
	Band 2 - Blue	458 - 523	10	
	Band 3 - Green	542 - 578	10	
	Band 4 - Red	650 - 680	10	
	Band 5 - Red Edge 1	698 - 713	20	
	Band 6 - Red Edge 2	733 - 748	20	
	Band 7 - Red Edge 3	773 - 793	20	
	Band 8 - Near Infrared (NIR)	784 - 875	10	
	Band 8A - Near Infrared (NIR Narrow)	865 - 885	20	
	Band 9 - Water Vapor	935 - 955	60	
	Band 10 - SWIR - Cirrus	1373 - 1390	60	
	Band 11 - SWIR 1	1565 - 1655	20	

 doi:10.20944/preprints202409.0674.v1

	Band 12 - SWIR 2	2100 - 2280	20	
Landsat 8 OLI	Band 1 - Coastal/ Aerosol	433 - 453	30	(https://www.usgs.gov/landsat-missions/landsat-collection-2-surface-reflectance)
	Band 2 - Blue	450 - 515	30	
	Band 3 - Green	525 - 600	30	
	Band 4 - Red	630 - 680	30	
	Band 5 - Near Infrared (NIR)	845 - 885	30	
	Band 6 - Shortwave Infrared 1 (SWIR 1)	1560 - 1660	30	
	Band 7 - Shortwave Infrared 2 (SWIR 2)	2100 - 2300	30	
	Band 8 - Panchromatic	500 - 680	15	
	Band 9 - Cirrus	1360 - 1390	30	
	Band 10 - Thermal Infrared 1 (TIRS 1)	10600 - 11190	100	
	Band 11 - Thermal Infrared 2 (TIRS 2)	11500 - 12510	100	

2.2.2. UAV Data

Remote sensing data collection involved ultra-high resolution UAV data captured via a DJI Phantom 4 Multispectral UAV from an altitude of 150 meters with base RTK-station. The P4 Multispectral (Table 2) consolidates the process of capturing data that provides insight into crop health and vegetation management. A spectral sunlight sensor catches solar irradiance, ensuring to maximize the accuracy and consistency of data collection. When combined with post-processed data, this information helps obtain the most accurate calculation of the vegetation indices (VI) (https://www.dji.com/global/p4-multispectral). The camera and images calibration were carried out during processing in Agisoft Metashape.

Table 2. The technical characteristics of UAV (P4-multispectral).

Specification	Description
Sensor Type	Complementary Metal Oxide Semiconductor (COMS)

 doi:10.20944/preprints202409.0674.v1

Number of Cameras	6
Spatial resolution (Multispectral)	Ground Sampling Distance (DGS) – 4cm(nadir)
Bands	RGB (combined from natural color), Multispectral (5 Bands)
Wavelength (by Bands)	1. Blue (approx. 450 nm) 2. Green (approx. 560 nm) 3. Red (approx. 650 nm) 4. Near Infrared (NIR) (approx. 700 nm) 5. Red Edge (approx. 740 nm)

2.3. Methods

2.3.1. Spectral Vegetation Indices

Remote sensing of natural grasslands and measuring their productivity primarily relies on vegetation indices. Vegetation spectral indices are a basic method for remote sensing data analysis. In this study, the following vegetation indices: NDVI, NDWI, GNDVI, GLI, EVI, DVI, SAVI, MSAVI, and GSAVI were used (Table 3).

Table 3. Applied spectral vegetation indices.

Index	Index name	Formula	Citation
NDVI	Normalized Difference Vegetation Index	$\frac{NIR - Red}{NIR + Red}$	[53]
NDWI	Normalized Difference Water Index	$\frac{Green - NIR}{Green + NIR}$	[54]
GNDVI	Green Normalized Difference Vegetation Index	$\frac{\text{NIR} - \text{Green}}{NIR + Green}$	[55]
GLI	Green Leaf Index	$\frac{2 * \text{Green} - \text{Red} - \text{Blue}}{2 * \text{Green} + \text{Red} + \text{Blue}}$	[56]
EVI	Enhanced Vegetation Index	$\frac{-2.5 * (\text{NIR} - \text{Red})}{NIR + 6 * Red - 7.5 * Blue + 1}$	[57]
DVI	Difference Vegetation Index	$NIR - Red$	[58]
SAVI	Soil Adjusted Vegetation Index	$\frac{1.5 * (NIR - Red)}{(NIR + Red + 0.5)}$	[59]
GSAVI	Green Soil Adjusted Vegetation Index	$\frac{1.5 * (NIR - Green)}{NIR + Green + 0.5}$	[60]
MSAVI	Modified Soil Adjusted Vegetation Index	$\frac{2 * \text{NIR} + 1 - \sqrt{(2 * NIR + 1)^2 - 8 * (\text{NIR} - \text{Red})}}{2}$	[60]

The most commonly used index to assess grassland vegetation and the state of biomass, and grass growth rates, is the Normalized Difference Vegetation Index (NDVI) presented by Rouse et al. (1974) [53,61] NDVI and the Enhanced Vegetation Index (EVI) have been widely used due to their

 doi:10.20944/preprints202409.0674.v1

strong correlation with plant growth status and spatial distribution density [57,62,63]. Huete et al. [64] demonstrated the high sensitivity of NDVI and EVI to the spatio-temporal variation of vegetation, land cover, and biophysical parameters. However, the applicability of NDVI can be limited [1] in sparse vegetation state due to significant soil background effects on green aboveground biomass estimation [65,66]. To address this limitation, Huete [59] proposed the Soil Adjusted Vegetation Index (SAVI), which incorporates a correction factor to minimize soil background effects [67]. Modified and improved versions of SAVI, such as the Modified Soil Adjusted Vegetation Index (MSAVI) and the Green Soil Adjusted Vegetation Index (GSAVI), have been developed to further reduce noise and soil background effects that affect NDVI [60,67,68]. In this context, the Difference Vegetation Index (DVI) is also noteworthy, as it separates vegetation from soil but does not account for atmospheric conditions and shadow presence [58]. The Green Leaf Index (GLI) is more accurate for distinguishing vegetation from the background and is also used for identifying single plant vegetation against different backgrounds [56]. Gitelson et al. [55] analyzed the sensitivity of visible reflectance to chlorophyll, noting that the green wavelength is more sensitive to chlorophyll than the red wavelength (used in NDVI), leading to the formation of the Green Normalized Difference Vegetation Index (GNDVI). This index achieved sufficient accuracy using the green channel to estimate vegetation cover. Considering that plant water content is also crucial for vegetation health, the Normalized Difference Water Index (NDWI) was calculated for the study area to evaluate the water content of the vegetation cover [54], as it is sensitive to changes in plant water content [69].

2.3.2. Spatial Correlation

To compare the effectiveness of RS data obtained from the different sources, images were collected to coincide with the peak of the growing season. UAV images were taken on June 29, 2023, followed by satellite images of the same area from Planet Scope on the same day, and from Landsat 8 OLI and Sentinel-2 on June 26 and 30, respectively. Since the acquired images have different spatial resolutions, resulting in the study area covering a different number of pixels, resampling was performed in the ArcGIS Pro environment using a Bilinear method based on the spatial resolution of the Planet Scope satellite images (3m). Downscaling and upscaling were implemented for the spatial resolution of the Landsat 8 OLI and Sentinel-2 data and the UAV data (P4 Multispectral), respectively. As a result, the same resolution and number of pixels were obtained for the study area across all four sources. Based on the resampled images, vegetation indices NDVI, NDWI, GNDVI, GLI, EVI, DVI, SAVI, MSAVI, and GSAVI were calculated for all images.

The normality distribution of data was checked using Anderson-Darling and Kolmogorov-Smirnov tests suitable for large datasets [70]. Both tests indicate that the data doesn't follow a normal distribution. Correlation analyses were carried out using the non-parametric Spearman correlation method, with significance levels $\alpha = 0.05$ (*), and $\alpha = 0.01$ (**), $P < 0,01$.

2.3.3. Trend Analysis

To analyze of short-term spatiotemporal changes in grassland vegetation monthly mean values of GLI, EVI, NDVI, and SAVI vegetation indices were used for May-July (vegetation peak) of 2018-2023, derived from LANDSAT, Sentinel, and Planet Scope satellites. These indices were chosen as indicators of the best correlation. Mann-Kendall statistical test was used for trend analysis [26,71] on Jupiter Notebook platform. This test was chosen because it is non-parametric and does not require a normal distribution of the data. Moreover, the test has low sensitivity to sharp time discontinuities due to inhomogeneous time series [72]. The original Mann-Kendall, Modified Mann-Kendall Test by Hamed and Rao (MKKH), Modified Mann-Kendall Test by Yue and Wang (MKKY), Pre-whitening Mann-Kendall Test PW), and Trend-Free Pre-whitening (TFPW) [73–76] trend tests, and Sen's Slope were used. According to [77], the trend is considered significant only if at least three of the five tests suggest a significant trend. As descriptive parameters of the Mann-Kendall test, Kendall's Tau and Z score were used. Kendall Tau, or Kendall's rank correlation coefficient, measures the monotonicity of the curve. Kendall's Tau ranges between -1 and 1; it is positive when the trend is increasing and negative when it is decreasing [78].

 doi:10.20944/preprints202409.0674.v1

The presence of statistically significant trends is assessed using the Z value. A statistically significant trend is determined by the absolute value of Z, $|Z| > 1,96$, which is the critical value of Z when $\alpha = 0,05$. The increasing or decreasing trend is indicated by a positive or negative Z score [72].

In addition to the Mann-Kendall method, Sen's slope was also used to estimate the slope of trend of the observed vegetation indices [79,80]. The Sen's slope model is suitable for qualitative characterization of trends over time [81,82]. The slope of Sen's slope is better suited for determining the magnitude of the trend. If the result of Sen's slope is positive, the time series has an increasing trend and vs [83].

3. Results

3.1. A Spatial Correlation Analysis of the Space - and UAV-Born Spectral Vegetation Indices

The correlation analysis shows significant correlation $\alpha = 0.01$** between all VIs derived from air and space born data, however with different intensity. As a result of the correlation analysis, we identified three levels of positive correlation strength: weak, medium, and strong, each representing a weak, noticeable but not strong, and strong relationship between the variables, respectively. Strong positive correlations were detected between the GLI index derived from UAV and GLI index from Planet Scope where r = 0.69, in the case of Landsat, r = 0.50 and r = 0.66 for Sentinel (Figure 2.)

Indices	*Satellite*	*Correlation(r)*
NDVI	PlanetScope	*0.50***
	Landsat 8	*0.40***
	Sentinel 2	*0.43***
GNDVI	PlanetScope	*0.14***
	Landsat 8	*0.04***
	Sentinel 2	*0.08***
GLI	PlanetScope	*0.69***
	Landsat 8	*0.50***
	Sentinel 2	*0.66***
SAVI	PlanetScope	*0.49***
	Landsat 8	*0.38***
	Sentinel 2	*0.43***
GSAVI	PlanetScope	*0.15***
	Landsat 8	*0.04***
	Sentinel 2	*0.09***
MSAVI	PlanetScope	*0.49***
	Landsat 8	*0.39***
	Sentinel 2	*0.43***
NWDI	PlanetScope	*0.14***
	Landsat 8	*0.01***
	Sentinel 2	*0.04***
DVI	PlanetScope	*0.43***
	Landsat 8	*0.34***
	Sentinel 2	*0.38***
EVI	PlanetScope	*0.61***
	Landsat 8	*0.54***
	Sentinel 2	*0.57***

Figure 2. Correlation between satellite (PlanetScope, Sentinel 2 and Landsat 8) and UAV data (at the 0.01** significance level).

 doi:10.20944/preprints202409.0674.v1

The SAVI correlation matrix shows moderate positive correlations with Planet Scope (r = 0.49) and Sentinel (r = 0.43), and a weak correlation with Landsat (r = 0.38). A similar trend is observed with MSAVI: moderate positive correlations with Planet Scope (r = 0.49) and Sentinel (r = 0.43), and a weak positive correlation with Landsat (r = 0.38). However, in the case of GSAVI vegetation index, UAV has a weak positive correlation with Planet Scope (r = 0.15) and no correlation with Landsat (r = 0.04) and Sentinel-2 (r = 0.09). The correlation of the NDWI derived UAV is weak with Planet Scope's NDWI (r = 0.14) and no correlation was observed with Landsat (r = 0.01) and Sentinel (r = 0.04).

As shown in the correlation analysis for NDVI, there is a strong correlation (r = 0.50) between UAV VIs and Planet Scope VIs, a moderate correlation (r = 0.40) between UAV VIs and Landsat VIs, and a moderate correlation (r = 0.43) between UAV VIs and Sentinel-2 VIs. For GNDVI, there are weak correlations among satellite VIs and UAV VIs. Specifically, weak positive correlations were observed between UAV VIs and Planet Scope (r = 0.14), Landsat (r = 0.04), and Sentinel (r = 0.08) VIs. Moderate positive correlations for DVI are observed with Planet Scope (r = 0.43), Landsat (r = 0.34), and Sentinel (r = 0.38). For EVI, strong positive correlations are detected: r = 0.61 with Planet Scope, r = 0.54 with Landsat, and r = 0.57 with Sentinel.

The analysis of the correlation tables shows that UAV VIs comparable to other sensors for vegetation monitoring, because in all cases, regardless of power and type, a significant correlation was observed (α = 0.01). In particularly GLI, EVI, and NDVI VIs stand out, in the case of which relatively strong correlations were obtained. However, the strength of the correlation indicates that there may be some differences in the information received due to sensor variations or other environmental factors.

3.2. Mann-Kendal Test for Temporal Analysis

The results of the statistical tests, show that the GLI, EVI, NDVI, and SAVI vegetation indices calculated for the Planet Scope satellite over a short time interval, from May to July 2018-2023, do not tend to change within a 95% confidence range (Figure 3).

	Indices	Time Series	MK			MKKH			MKKY			PW			TFPW			Sen's slope	Trend (alpha = 0.05)
			P	Z	Tau	P	Z	Tau	P	Z	Tau	P	Z	Tau	P	Z	Tau		
Planet Scope	GLI	May	0.259656	1.127204	0.466667	0.259656	1.127204	0.466667	0.027109	2.20994	0.466667	1	0	0	0.462433	0.734847	0.4	0.031774398	no trend
		June	0.259656	1.127204	0.466667	0.259656	1.127204	0.466667	0.001435	3.187597	0.466667	0.462433	0.734847	0.4	0.806496	0.244949	0.2	0.018492993	no trend
		July	0.45237	0.751469	0.333333	0.45237	0.751469	0.333333	0.052026	1.942921	0.333333	0.220671	1.224745	0.6	0.220671	1.224745	0.6	0.026915202	no trend
	EVI	May	0.259656	-1.1272	-0.46667	0.259656	-1.1272	-0.46667	0.005734	-2.76261	-0.46667	0.220671	-1.22474	-0.6	0.462433	-0.73485	-0.4	-0.101395335	no trend
		June	0.45237	-0.75147	-0.33333	0.45237	-0.75147	-0.33333	0.098056	-1.65435	-0.33333	0.220671	-1.22474	-0.6	0.462433	-0.73485	-0.4	-0.08012681	no trend
		July	0.707114	-0.37573	-0.2	0.707114	-0.37573	-0.2	0.415956	-0.81346	-0.2	0.806496	-0.24495	-0.2	0.806496	-0.24495	-0.2	-0.093031178	no trend
	NDVI	May	1	0	-0.06667	1	0	-0.06667	1	0	-0.06667	0.462433	-0.73485	-0.4	1	0	0	-0.024994207	no trend
		June	0.132855	-1.50294	-0.6	0.132855	-1.50294	-0.6	0.002497	-3.0237	-0.6	0.462433	-0.73485	-0.4	0.462433	-0.73485	-0.4	-0.028591617	no trend
		July	0.707114	-0.37573	-0.2	0.707114	-0.37573	-0.2	0.473293	-0.71713	-0.2	0.806496	-0.24495	-0.2	0.806496	-0.24495	-0.2	-0.026520961	no trend
	SAVI	May	0.707114	-0.37573	-0.2	0.465209	-0.7303	-0.2	0.302985	-1.03005	-0.2	0.462433	-0.73485	-0.4	0.806496	-0.24495	-0.2	-0.03746088	no trend
		June	0.132855	-1.50294	-0.6	0.132855	-1.50294	-0.6	0.003158	-2.95189	-0.6	0.462433	-0.73485	-0.4	0.462433	-0.73485	-0.4	-0.04288168	no trend
		July	0.707114	-0.37573	-0.2	0.707114	-0.37573	-0.2	0.473304	-0.71711	-0.2	0.806496	-0.24495	-0.2	0.806496	-0.24495	-0.2	-0.03976658	no trend
Sentinel 2	GLI	May	0.024171	-2.25441	-0.86667	0.024171	-2.25441	-0.86667	2.85E-06	-4.6815	-0.86667	0.086411	-1.71464	-0.8	0.027486	-2.20454	-1	-0.010325	decreasing
		June	0.707114	-0.37573	-0.2	0.707114	-0.37573	-0.2	0.477475	-0.71037	-0.2	1	0	0	0.806496	0.244949	0.2	-0.005833333	no trend
		July	1	0	-0.06667	1	0	-0.06667	1	0	-0.06667	1	0	0	1	0	0	-0.001966667	no trend
	EVI	May	0.45237	-0.75147	-0.33333	0.45237	-0.75147	-0.33333	0.053537	-1.93056	-0.33333	0.220671	-1.22474	-0.6	0.220671	-1.22474	-0.6	-0.087412698	no trend
		June	1	0	-0.06667	1	0	-0.06667	1	0	-0.06667	0.806496	0.244949	0.2	0.806496	0.244949	0.2	-0.023416667	no trend
		July	0.45237	0.751469	0.333333	0.45237	0.751469	0.333333	0.094504	1.672104	0.333333	0.806496	0.244949	0.2	0.806496	0.244949	0.2	0.03716	no trend
	NDVI	May	0.024171	-2.25441	-0.86667	0.024171	-2.25441	-0.86667	3.83E-08	-5.49837	-0.86667	0.027486	-2.20454	-1	0.027486	-2.20454	-1	-0.02765	decreasing
		June	0.45237	-0.75147	-0.33333	0.45237	-0.75147	-0.33333	0.136498	-1.48896	-0.33333	1	0	0	0.806496	-0.24495	-0.2	-0.014777778	no trend
		July	1	0	-0.06667	1	0	-0.06667	1	0	-0.06667	1	0	0	1	0	0	-0.004027273	no trend
	SAVI	May	0.024171	-2.25441	-0.86667	0.024171	-2.25441	-0.86667	4.51E-08	-5.46971	-0.86667	0.027486	-2.20454	-1	0.027486	-2.20454	-1	-0.0415	decreasing
		June	0.45237	-0.75147	-0.33333	0.45237	-0.75147	-0.33333	0.136087	-1.49052	-0.33333	1	0	0	0.806496	-0.24495	-0.2	-0.022322222	no trend
		July	1	0	-0.06667	1	0	-0.06667	1	0	-0.06667	1	0	0	1	0	0	-0.006042424	no trend
Landsat 8	GLI	May	0.462433	0.734847	0.4	0.220671	1.224745	0.4	0.124408	1.53653	0.4	0.734095	0.339683	0.333333	0.30818	1.019049	0.666667	0.0004	no trend
		June	0.45237	0.751469	0.333333	0.45237	0.751469	0.333333	0.054951	1.919263	0.333333	0.462433	0.734847	0.4	0.462433	0.734847	0.4	0.0034	no trend
		July	0.259656	1.127204	0.466667	0.259656	1.127204	0.466667	0.00589	2.753856	0.466667	0.220671	1.224745	0.6	0.462433	0.734847	0.4	0.0021	no trend
	EVI	May	0.462433	-0.73485	-0.4	0.462433	-0.73485	-0.4	0.052744	-1.93701	-0.4	0.734095	-0.33968	-0.33333	0.089429	-1.69842	-1	-0.00385	no trend
		June	1	0	-0.06667	1	0	-0.06667	1	0	-0.06667	0.806496	0.244949	0.2	0.806496	0.244949	0.2	-0.0008	no trend
		July	0.45237	0.751469	0.333333	0.45237	0.751469	0.333333	0.096562	1.661757	0.333333	0.220671	1.224745	0.6	0.220671	1.224745	0.6	0.004	no trend
	NDVI	May	0.806496	0.244949	0.2	0.683091	0.408248	0.2	0.573202	0.563342	0.2	0.089429	1.698416	1	0.30818	1.019049	0.666667	0.002383333	no trend
		June	0.1806	1.338911	0.533333	0.1806	1.338911	0.533333	0.007036	2.695154	0.533333	0.462433	0.734847	0.4	0.462433	0.734847	0.4	0.03275	no trend
		July	0.45237	0.751469	0.333333	0.45237	0.751469	0.333333	0.074091	1.786048	0.333333	0.462433	0.734847	0.4	0.806496	0.244949	0.2	0.0057	no trend
	SAVI	May	1	0	0	1	0	0	1	0	0	0.089429	1.698416	1	0.089429	1.698416	1	-0.00035	no trend
		June	0.259656	1.127204	0.466667	0.259656	1.127204	0.466667	0.008706	2.62339	0.466667	0.462433	0.734847	0.4	0.462433	0.734847	0.4	0.01475	no trend
		July	0.707114	0.375735	0.2	0.707114	0.375735	0.2	0.405036	0.832662	0.2	0.462433	0.734847	0.4	0.462433	0.734847	0.4	0.00625	no trend

Figure 3. Trend analysis of best correlated vegetation indices received from different sources.

According to the MKKY test, the NDVI and SAVI values show a significant decreasing trend in June at the α = 0.05 significance level, as indicated by P < α (P = 0.002) and Z = -3.023 (NDVI) and P = 0.03, Z = -2.951 (SAVI), with |Z| > 1.96 correspondingly. The GLI index also shows a significant trend revealed by MKKY test in May and June, were P = 0.027 (P < α), Z = 2.209 (|Z| < 1.96), Tau = 0,466

 doi:10.20944/preprints202409.0674.v1

(moderate increasing trend), Sen's slope = 0.031 (increasing trend [83,84]), and P = 0.027 (P < α), Z = 2.043 (|Z| < 1.96), Tau = 0,466 (moderate increasing trend), Sen's slope = 0.025 (increasing trend) respectively. Although several significant trends were observed, no consistent trend was detected for GLI, EVI, NDVI, and SAVI vegetation indices from May to June 2018-2023. This is because only one of the tests (MKKY) recorded trends where Tau indicates a moderate decreasing trend (-0.6 to 0) for all indices from May to July, except for GLI, from 0 to 0.466.

The results of the statistical tests of vegetation indices obtained from SENTINEL-2 satellite images for 2018-2023 (May-July), depict fixed changes for GLI, NDVI, and SAVI vegetation indices. A significant trend of GLI values is observed in May, confirmed by the MK, MKKH, MKKY and TFPW tests at the 0.05 significance level. The MK and MKKH tests show P = 0.024, with P < α, and |Z| = 2.254 |Z| > 1.96. However, Z = -2.254 indicating a decreasing trend, which is supported by the Tau value of -0.866. According to the MKKY P = 2.85E-06 < 0.05; Z = -4.681, Tau = -0.866. The TFPW test shows P = 0.027, P < α, with Z = -2.204 and Tau = -1, also indicating a decreasing trend. Thus, a significant decreasing trend is observed for GLI for short time period (2018-2023) indicated by four tests, expect PW. For the EVI as well as in the case of Planet Scope no changes were observed. A trend of the changes of NDVI index was observed only in May by all applied tests. In May, the original MK and MKKH tests detected a significant trend at the α = 0.05 significance level, with P =0.024 P < α, Z = -2.254 (|Z| > 1.96), and Tau = -0.866. With the MKKY test P = 3.83E-08, P < α, Z = -5.498, and Tau = -0.866, indicating a significant decreasing trend. Descriptive parameters of the PW and TFPW tests with the same values: P = 0.027, Z = -2.205, Tau = -1, show a significant decreasing trend. The same values of P and Z for SAVI were recorded by the four tests, as was in case of the NDVI, except for MKKY test, where P = 4.508E-08 and Z = -5.469 and which proves the significant decreasing trend.

No significant increasing or decreasing trends were observed for GLI, EVI, NDVI, and SAVI vegetation indices obtained from Landsat satellite images between May and July of 2018-2023. An increasing trend for GLI was observed in July, recorded only by the MKKY test, according to which P = 0.005 < α and Z = 2.753 > 1,96. According to the MKKY test, a statistically significant trend in NDVI was observed only in June, where P = 0.007, P < α, |Z| = 2.695 > 1.96, Tau = 0.533 (moderate increasing), Sen's slope = 0.032 (indicating an increasing trend). No trend in EVI index values was registered by any of the tests. The MKKY test detected a statistically significant trend for SAVI values at the α = 0.05 significance level in June, with P = 0.008, Z = 2.623, |Z| > 1.96, indicating an increasing trend. This trend is further supported by the Tau value (0.466) indicating moderate increase. However, only one test recorded a trend means there is no trend for the studied period. Thus, according to the Mann-Kendall tests, only Sentinel 2 data show decreasing trend.

SEN slope estimator shows different results compared with MK tests. Generally, we have indicated similar negative directions of the values for Planet (averaged -0.03 year^{-1}) and Sentinel (averaged -0.01 year^{-1}) based VIs, which is not even close to those received for Landsat 8 not in direction nor in values (average 0.005 year^{-1}).

4. Discussion

Our study was targeted to explore multisource remote sensing capacities for assessing and monitoring mountainous natural grasslands in Armenia. A list of spectral indices (Table 3), which had proven to be valuable tools in describing spatial and temporal variability of biomass [34,85] was applied to compare multisource space-born remote sensing data (Planet Scope, Sentinel-2 and Landsat 8) with air-born (UAV) data using Spearmen correlation analysis. The aim was to assess the capability of each space platform for analyzing the trend of short-term spatial-temporal changes of Armenian grasslands for May-July 2018-2023. It is noteworthy that in our study air born (UAV) remote sensing was applied as validation tool. This approach in known for mapping complex vegetation of peatlands [33]. The correlations between UAV and satellite-based indices were positive, but distinguished with the different correlation strengths. Strong positive correlations were observed with the NDVI, GLI and EVI indices; Moderate between SAVI, MSAVI and DVI; and Weak correlation between NDWI, GNDVI and GSAVI indices. Additionally, high correlations of UAV were with Planet Scope, after Sentinel 2 and Landsat 8 was registered. The correlation analysis confirms

 doi:10.20944/preprints202409.0674.v1

that UAV VIs comparable to the space-born multisensory data for monitoring mountain grasslands, because in all cases, a significant positive correlation $p < 0.01$ (**) was observed. The spatial correlation figured out four main spectral indices (NDVI, GLI, EVI and SAVI), which shows strong significant correlation with those calculated from UAV data. Afterwards, Mann-Kendall tests (MK, MKKH, MKKY, PW, TFPW) were applied for trend analysis. According to all five Mann-Kendall tests among the studied platforms only three Sentinel-2 based indices (NDVI, GLI, and SAVI) show decreasing trend for May-July 2018-2023. So, Sentinel-2 shows more consistent and frequent detection of significant trends across vegetation indices. It is important to note that all changes which prove a significant decreasing trend for the studied short period are observed only in May.

If we consider Sen's Slope as an individual estimator, well applied for the trend analysis based on short term databases and, which applied for different studies [79–81] we can indicate that according to Sen's Slope the Planet Scope and Sentinel-2 based estimations show decreasing trend, which according to MK tests were observed for Sentinel-2 based VIs only in May. It gives a food for thought: Sens's slope could be more robust for our case than MK tests.

5. Conclusions

As can be seen from the analysis in the short term (2018-2023) changes assessment of the state of mountain natural grasslands, although the high-resolution data from Planet Scope provide detailed information, the medium-resolution images from Sentinel and Landsat sensors can be effectively used in the assessment of grassland state. Planet Scope satellite data were taken as a reference due to the high spatial resolution to understand the effectiveness of using data from medium-resolution Landsat and Sentinel satellites for short-term trend analysis. Both Landsat and Sentinel data show potential for monitoring short-term changes when compared to high-resolution Planet Scope data. However, Sentinel-2 data seem to have an obscurely better alignment. Apart from the fact that the Sentinel 2 is closer to the Planet Scope due to its spatial resolution (10m) than the Landsat 8 (30m), which increases the effectiveness of the Sentinel 2 application, the analysis results further confirm that. In addition, Sentinel-2 is an open-source data and all these make Sentinel-2 a reliable and effective tool for detailed and accurate monitoring of grassland biomass in mountainous small areas.

According to Sen's slope result, a well-expressed relationship between Sentinel 2 and Planet Scope is clearly visible, which was expected due to the spatial resolution. Thus, according to the results for Planet Scope and Sentinel 2 the trends are biased to decrease, but for Landsat 8 is the vice versa.

Therefore, it cannot be stated with certainty that the small area under consideration showed an increasing or decreasing trend over a short period of time. In order to have an even clearer picture of the situation, it is necessary to study a wider spatial and temporal series and include climatic data. Moreover, there are several factors that should be considered in our future research such as human impact on the grasslands, and also in situ data should be included which will enable us to make a quantitative and qualitative analysis of above ground biomass.

Author Contributions: "Conceptualization, G.A., V.M., A.M., and Sh.A.; methodology, G.A., V.M., A.M., Sh.A.; validation, G.A., V.M., and A. Kh.; formal analysis, G.A., V.M., and A. Kh.; investigation, G.A., V.M., A.M., and Sh.A.; resources, A.M. and A. Kh.; data curation, G.A., A.Kh., A.M., and V.M.; writing—original draft preparation, G.A.; writing—review and editing, Sh.A. and V.M.; visualization, G.A., A. Kh., and A.M.; supervision, Sh.A. and V.M.; project administration, G.A. and Sh.A.; funding acquisition, G.A. All authors have read and agreed to the published version of the manuscript.

Funding: The work was implemented in frames of No 22AA-1E021 project funded by the Science Committee/Higher Education and Science Committee of the Ministry of Education, Science, Culture and Sport of RA.

Acknowledgments: The research was conducted in the Center for Ecological-Noosphere Studies NAS RA (CENS) and authors would like to acknowledge the administration for existing facilities to conduct this research. Authors also acknowledge the Authorities of Nerkin Sasnashen rural community for dedicated support during field survey. Finaly, the research was funded by Science Committee/Higher Education and Science Committee of the Ministry of Education, Science, Culture and Sport of RA.

Conflicts of Interest: The authors declare no conflicts of interest.

References

1. Wang, Z.; Ma, Y.; Zhang, Y.; Shang, J. Review of Remote Sensing Applications in Grassland Monitoring. *Remote Sens (Basel)* 2022, *14*.
2. *Grasslands: Developments Opportunities Perspectives*; Reynolds, S.G., Frame, J., Eds.; CRC Press, 2019; ISBN 9780429187872.
3. Reinermann, S.; Asam, S.; Kuenzer, C. Remote Sensing of Grassland Production and Management-A Review. *Remote Sens (Basel)* 2020, *12*.
4. Bar-On, Y.M.; Phillips, R.; Milo, R. The Biomass Distribution on Earth. *Proc Natl Acad Sci U S A* **2018**, *115*, 6506–6511, doi:10.1073/pnas.1711842115.
5. Erb, K.H.; Kastner, T.; Plutzar, C.; Bais, A.L.S.; Carvalhais, N.; Fetzel, T.; Gingrich, S.; Haberl, H.; Lauk, C.; Niedertscheider, M.; et al. Unexpectedly Large Impact of Forest Management and Grazing on Global Vegetation Biomass. *Nature* **2018**, *553*, 73–76, doi:10.1038/nature25138.
6. *Grassland Productivity and Ecosystem Services*; Lemaire, G., Hodgson, J., Chabbi, A., Eds.; CABI: UK, 2011; ISBN 9781845938093.
7. Dusseux, P.; Guyet, T.; Pattier, P.; Barbier, V.; Nicolas, H. Monitoring of Grassland Productivity Using Sentinel-2 Remote Sensing Data. *International Journal of Applied Earth Observation and Geoinformation* **2022**, *111*, 102843, doi:10.1016/j.jag.2022.102843.
8. Davidson, A.D.; Detling, J.K.; Brown, J.H. Ecological Roles and Conservation Challenges of Social, Burrowing, Herbivorous Mammals in the World's Grasslands. *Front Ecol Environ* **2012**, *10*, 477–486, doi:10.1890/110054.
9. Sloat, L.L.; Gerber, J.S.; Samberg, L.H.; Smith, W.K.; Herrero, M.; Ferreira, L.G.; Godde, C.M.; West, P.C. Increasing Importance of Precipitation Variability on Global Livestock Grazing Lands. *Nat Clim Chang* **2018**, *8*, 214–218, doi:10.1038/s41558-018-0081-5.
10. Teixeira, R.F.M.; Barão, L.; Morais, T.G.; Domingos, T. "BalSim": A Carbon, Nitrogen and Greenhouse Gas Mass Balance Model for Pastures. *Sustainability (Switzerland)* **2019**, *11*, doi:10.3390/su11010053.
11. Teixeira, R.F.M.; Morais, T.G.; Domingos, T. A Practical Comparison of Regionalized Land Use and Biodiversity Life Cycle Impact Assessment Models Using Livestock Production as a Case Study. *Sustainability (Switzerland)* **2018**, *10*, doi:10.3390/su10114089.
12. Morais, T.G.; Teixeira, R.F.M.; Figueiredo, M.; Domingos, T. The Use of Machine Learning Methods to Estimate Aboveground Biomass of Grasslands: A Review. *Ecol Indic* **2021**, *130*, 108081, doi:10.1016/j.ecolind.2021.108081.
13. Peeters, A. Importance, Evolution, Environmental Impact and Future Challenges of Grasslands and Grassland-based Systems in Europe. *Grassl Sci* **2009**, *55*, 113–125, doi:10.1111/j.1744-697X.2009.00154.x.
14. Soussana, J.; Lüscher, A. Temperate Grasslands and Global Atmospheric Change: A Review. *Grass and Forage Science* **2007**, *62*, 127–134, doi:10.1111/j.1365-2494.2007.00577.x.
15. Lu, D.; Batistella, M.; Mausel, P.; Moran, E. Mapping and Monitoring Land Degradation Risks in the Western Brazilian Amazon Using Multitemporal Landsat TM/ETM+ Images. *Land Degrad Dev* **2007**, *18*, 41–54, doi:10.1002/ldr.762.
16. Junges, A.H.; Bremm, C.; Fontana, D.C.; Oliveira, C.A.O. de; Schaparini, L.P.; Carvalho, P.C. de F. Temporal Profiles of Vegetation Indices for Characterizing Grazing Intensity on Natural Grasslands in Pampa Biome. *Sci Agric* **2016**, *73*, 332–337, doi:10.1590/0103-9016-2015-0213.
17. Zhang, Z.; Feng, Z.; Zhang, H.; Zhao, J.; Yu, S.; Du, W. Spatial Distribution of Grassland Fires at the Regional Scale Based on the MODIS Active Fire Products. *Int J Wildland Fire* **2017**, *26*, 209, doi:10.1071/WF16026.
18. Lu, B.; He, Y.; Tong, A. Evaluation of Spectral Indices for Estimating Burn Severity in Semiarid Grasslands. *Int J Wildland Fire* **2016**, *25*, 147, doi:10.1071/WF15098.
19. Ma, Q.; Kuang, W.; Liu, Z.; Hu, F.; Qian, J.; Liu, B.; Zhu, J.; Cao, C.; Wu, J.; Li, X.; et al. Spatial Pattern of Different Component Carbon in Varied Grasslands of Northern China. *Geoderma* **2017**, *303*, 27–36, doi:10.1016/j.geoderma.2017.05.010.
20. Lyu, X.; Li, X.; Dang, D.; Dou, H.; Wang, K.; Lou, A. Unmanned Aerial Vehicle (UAV) Remote Sensing in Grassland Ecosystem Monitoring: A Systematic Review. *Remote Sens (Basel)* 2022, *14*.
21. Li, Z.; Li, X.; Chen, L.; Li, R.; Deng, F.; Zhang, M.; Wen, L. Carbon Flux and Soil Organic Carbon Content and Density of Different Community Types in a Typical Steppe Ecoregion of Xilin Gol in Inner Mongolia, China. *J Arid Environ* **2020**, *178*, 104155, doi:10.1016/j.jaridenv.2020.104155.
22. Lyu, X.; Li, X.; Gong, J.; Wang, H.; Dang, D.; Dou, H.; Li, S.; Liu, S. Comprehensive Grassland Degradation Monitoring by Remote Sensing in Xilinhot, Inner Mongolia, China. *Sustainability* **2020**, *12*, 3682, doi:10.3390/su12093682.
23. HOPKINS, A.; WILKINS, R.J. Temperate Grassland: Key Developments in the Last Century and Future Perspectives. *J Agric Sci* **2006**, *144*, 503–523, doi:10.1017/S0021859606006496.

24. Bengtsson, J.; Bullock, J.M.; Egoh, B.; Everson, C.; Everson, T.; O'Connor, T.; O'Farrell, P.J.; Smith, H.G.; Lindborg, R. Grasslands—More Important for Ecosystem Services than You Might Think. *Ecosphere* **2019**, *10*, doi:10.1002/ecs2.2582.
25. Bazzo, C.O.G.; Kamali, B.; Hütt, C.; Bareth, G.; Gaiser, T. A Review of Estimation Methods for Aboveground Biomass in Grasslands Using UAV. *Remote Sens (Basel)* 2023, *15*.
26. Muradyan, V.; Asmaryan, S.; Ayvazyan, G.; Dell'Acqua, F. Multidecadal Trend Analysis of Armenian Mountainous Grassland and Its Relationship to Climate Change Using Multi-Sensor NDVI Time-Series. *Geosciences (Switzerland)* **2022**, *12*, doi:10.3390/geosciences12110412.
27. Nestola, E.; Calfapietra, C.; Emmerton, C.; Wong, C.; Thayer, D.; Gamon, J. Monitoring Grassland Seasonal Carbon Dynamics, by Integrating MODIS NDVI, Proximal Optical Sampling, and Eddy Covariance Measurements. *Remote Sens (Basel)* **2016**, *8*, 260, doi:10.3390/rs8030260.
28. Ali, I.; Cawkwell, F.; Dwyer, E.; Barrett, B.; Green, S. Satellite Remote Sensing of Grasslands: From Observation to Management. *Journal of Plant Ecology* **2016**, *9*, 649–671, doi:10.1093/jpe/rtw005.
29. Zhou, Y.; Liu, T.; Batelaan, O.; Duan, L.; Wang, Y.; Li, X.; Li, M. Spatiotemporal Fusion of Multi-Source Remote Sensing Data for Estimating Aboveground Biomass of Grassland. *Ecol Indic* **2023**, *146*, 109892, doi:10.1016/j.ecolind.2023.109892.
30. Lussem, U.; Bolten, A.; Menne, J.; Gnyp, M.L.; Schellberg, J.; Bareth, G. Estimating Biomass in Temperate Grassland with High Resolution Canopy Surface Models from UAV-Based RGB Images and Vegetation Indices. *J Appl Remote Sens* **2019**, *13*, 1, doi:10.1117/1.jrs.13.034525.
31. Liaghat, S.; Balasundram, S.K. A Review: The Role of Remote Sensing in Precision Agriculture. *American Journal of Agricultural and Biological Science* 2010, *5*, 50–55.
32. Li, C.; Han, W.; Peng, M. Improving the Spatial and Temporal Estimating of Daytime Variation in Maize Net Primary Production Using Unmanned Aerial Vehicle-Based Remote Sensing. *International Journal of Applied Earth Observation and Geoinformation* **2021**, *103*, 102467, doi:10.1016/j.jag.2021.102467.
33. Cottrell, B.; Kalacska, M.; Arroyo-Mora, J.-P.; Lucanus, O.; Inamdar, D.; Løke, T.; Soffer, R.J. Limitations of a Multispectral UAV Sensor for Satellite Validation and Mapping Complex Vegetation. *Remote Sens (Basel)* **2024**, *16*, 2463, doi:10.3390/rs16132463.
34. Matese, A.; Toscano, P.; Di Gennaro, S.; Genesio, L.; Vaccari, F.; Primicerio, J.; Belli, C.; Zaldei, A.; Bianconi, R.; Gioli, B. Intercomparison of UAV, Aircraft and Satellite Remote Sensing Platforms for Precision Viticulture. *Remote Sens (Basel)* **2015**, *7*, 2971–2990, doi:10.3390/rs70302971.
35. Dusseux, P.; Hubert-Moy, L.; Corpetti, T.; Vertès, F. Evaluation of SPOT Imagery for the Estimation of Grassland Biomass. *International Journal of Applied Earth Observation and Geoinformation* **2015**, *38*, 72–77, doi:10.1016/j.jag.2014.12.003.
36. Zheng, H.; Zhou, X.; He, J.; Yao, X.; Cheng, T.; Zhu, Y.; Cao, W.; Tian, Y. Early Season Detection of Rice Plants Using RGB, NIR-G-B and Multispectral Images from Unmanned Aerial Vehicle (UAV). *Comput Electron Agric* **2020**, *169*, 105223, doi:10.1016/j.compag.2020.105223.
37. Zeng, Y.; Hao, D.; Huete, A.; Dechant, B.; Berry, J.; Chen, J.M.; Joiner, J.; Frankenberg, C.; Bond-Lamberty, B.; Ryu, Y.; et al. Optical Vegetation Indices for Monitoring Terrestrial Ecosystems Globally. *Nat Rev Earth Environ* **2022**, *3*, 477–493, doi:10.1038/s43017-022-00298-5.
38. Wang, J.; Zhen, J.; Hu, W.; Chen, S.; Lizaga, I.; Zeraatpisheh, M.; Yang, X. Remote Sensing of Soil Degradation: Progress and Perspective. *International Soil and Water Conservation Research* **2023**, *11*, 429–454, doi:10.1016/j.iswcr.2023.03.002.
39. FRANKLIN, K.; MOLINA-FREANER, F. Consequences of Buffelgrass Pasture Development for Primary Productivity, Perennial Plant Richness, and Vegetation Structure in the Drylands of Sonora, Mexico. *Conservation Biology* **2010**, *24*, 1664–1673, doi:10.1111/j.1523-1739.2010.01540.x.
40. Gao, Q.; Schwartz, M.; Zhu, W.; Wan, Y.; Qin, X.; Ma, X.; Liu, S.; Williamson, M.; Peters, C.; Li, Y. Changes in Global Grassland Productivity during 1982 to 2011 Attributable to Climatic Factors. *Remote Sens (Basel)* **2016**, *8*, 384, doi:10.3390/rs8050384.
41. Gu, Y.; Wylie, B.K. Developing a 30-m Grassland Productivity Estimation Map for Central Nebraska Using 250-m MODIS and 30-m Landsat-8 Observations. *Remote Sens Environ* **2015**, *171*, 291–298, doi:10.1016/j.rse.2015.10.018.
42. Kath, J.; Le Brocque, A.F.; Reardon-Smith, K.; Apan, A. Remotely Sensed Agricultural Grassland Productivity Responses to Land Use and Hydro-Climatic Drivers under Extreme Drought and Rainfall. *Agric For Meteorol* **2019**, *268*, 11–22, doi:10.1016/j.agrformet.2019.01.007.
43. Qamer, F.; Xi, C.; Abbas, S.; Murthy, M.; Ning, W.; Anming, B. An Assessment of Productivity Patterns of Grass-Dominated Rangelands in the Hindu Kush Karakoram Region, Pakistan. *Sustainability* **2016**, *8*, 961, doi:10.3390/su8090961.
44. Reeves, M.C.; Baggett, L.S. A Remote Sensing Protocol for Identifying Rangelands with Degraded Productive Capacity. *Ecol Indic* **2014**, *43*, 172–182, doi:10.1016/j.ecolind.2014.02.009.

45. Yin, F.; Deng, X.; Jin, Q.; Yuan, Y.; Zhao, C. The Impacts of Climate Change and Human Activities on Grassland Productivity in Qinghai Province, China. *Front Earth Sci* **2014**, *8*, 93–103, doi:10.1007/s11707-013-0390-y.
46. Asmaryan, Sh.,; Mezhunts, B., Mapping and Assessing the Community Grasslands and Developing a Grazing Scheme; Yerevan, 2011;
47. Tepanosyan, G. Applicability of Linear Spectral Unmixing in Delineating Potential Erosion Areas in Highland Pastures (Case Study of Nerkin Sasoonashen Rural Community). *Agroscience, 2016, No. 1-2* **2019**, 44–49.
48. Ayvazyan, G.; Asmaryan, S. SATELLITE REMOTE SENSING FOR ASSESSING THE SPATIOTEMPORAL CHANGES OF THE ECOLOGICAL STATE OF THE AGRICULTURAL LANDS IN ARMENIA. *The International Archives of the Photogrammetry, Remote Sensing and Spatial Information Sciences* **2023**, *XLVIII-1/W2-2023*, 1325–1330, doi:10.5194/isprs-archives-XLVIII-1-W2-2023-1325-2023.
49. Zhao, G.; Zhang, Y.; Tan, J.; Li, C.; Ren, Y. A Data Fusion Modeling Framework for Retrieval of Land Surface Temperature from Landsat-8 and MODIS Data. *Sensors* **2020**, *20*, 4337, doi:10.3390/s20154337.
50. Zhang, H.K.; Huang, B.; Zhang, M.; Cao, K.; Yu, L. A Generalization of Spatial and Temporal Fusion Methods for Remotely Sensed Surface Parameters. *Int J Remote Sens* **2015**, *36*, 4411–4445, doi:10.1080/01431161.2015.1083633.
51. Zhu, X.; Cai, F.; Tian, J.; Williams, T. Spatiotemporal Fusion of Multisource Remote Sensing Data: Literature Survey, Taxonomy, Principles, Applications, and Future Directions. *Remote Sens (Basel)* **2018**, *10*, 527, doi:10.3390/rs10040527.
52. "Centre of Geodesy and Cartography" SNCO *National Atlas of Armenia*; "Centre of Geodesy and Cartography" SNCO: Yerevan, 2007; Vol. 1;.
53. Edirisinghe, A.; Clark, D.; Waugh, D. Spatio-Temporal Modelling of Biomass of Intensively Grazed Perennial Dairy Pastures Using Multispectral Remote Sensing. *International Journal of Applied Earth Observation and Geoinformation* **2012**, *16*, 5–16, doi:10.1016/j.jag.2011.11.006.
54. Ji, L.; Zhang, L.; Wylie, B. Analysis of Dynamic Thresholds for the Normalized Difference Water Index. *Photogramm Eng Remote Sensing* **2009**, *75*, 1307–1317, doi:10.14358/PERS.75.11.1307.
55. Gitelson, A.A.; Kaufman, Y.J.; Merzlyak, M.N. Use of a Green Channel in Remote Sensing of Global Vegetation from EOS-MODIS. *Remote Sens Environ* **1996**, *58*, 289–298, doi:10.1016/S0034-4257(96)00072-7.
56. Bassine, F.Z.; Errami, A.; Khaldoun, M. Vegetation Recognition Based on UAV Image Color Index. In Proceedings of the 2019 IEEE International Conference on Environment and Electrical Engineering and 2019 IEEE Industrial and Commercial Power Systems Europe (EEEIC / I&CPS Europe); IEEE, June 2019; pp. 1–4.
57. Zhang, W.; Yang, X.; Manlike, A.; Jin, Y.; Zheng, F.; Guo, J.; Shen, G.; Zhang, Y.; Xu, B. Comparative Study of Remote Sensing Estimation Methods for Grassland Fractional Vegetation Coverage – a Grassland Case Study Performed in Ili Prefecture, Xinjiang, China. *Int J Remote Sens* **2019**, *40*, 2243–2258, doi:10.1080/01431161.2018.1508918.
58. Mokarram, M.; Hojjati, M.; Roshan, G.; Negahban, S. Modeling the Behavior of Vegetation Indices in the Salt Dome of Korsia in North-East of Darab, Fars, Iran. *Model Earth Syst Environ* **2015**, *1*, 27, doi:10.1007/s40808-015-0029-y.
59. Huete, A.R. A Soil-Adjusted Vegetation Index (SAVI). *Remote Sens Environ* **1988**, *25*, 295–309, doi:10.1016/0034-4257(88)90106-X.
60. Ren, H.; Zhou, G.; Zhang, F. Using Negative Soil Adjustment Factor in Soil-Adjusted Vegetation Index (SAVI) for Aboveground Living Biomass Estimation in Arid Grasslands. *Remote Sens Environ* **2018**, *209*, 439–445, doi:10.1016/j.rse.2018.02.068.
61. Hill, M.J.; Donald, G.E.; Hyder, M.W.; Smith, R.C.G. Estimation of Pasture Growth Rate in the South West of Western Australia from AVHRR NDVI and Climate Data. *Remote Sens Environ* **2004**, *93*, 528–545, doi:10.1016/j.rse.2004.08.006.
62. Ye, H.; Huang, X.; Luo, G.; Wang, J.; Zhang, M.; Wang, X. Improving Remote Sensing-Based Net Primary Production Estimation in the Grazed Land with Defoliation Formulation Model. *J Mt Sci* **2019**, *16*, 323–336, doi:10.1007/s11629-018-5200-2.
63. Karimi, S.; Sadraddini, A.A.; Nazemi, A.H.; Xu, T.; Fard, A.F. Generalizability of Gene Expression Programming and Random Forest Methodologies in Estimating Cropland and Grassland Leaf Area Index. *Comput Electron Agric* **2018**, *144*, 232–240, doi:10.1016/j.compag.2017.12.007.
64. Huete, A.; Didan, K.; Miura, T.; Rodriguez, E.P.; Gao, X.; Ferreira, L.G. Overview of the Radiometric and Biophysical Performance of the MODIS Vegetation Indices. *Remote Sens Environ* **2002**, *83*, 195–213, doi:10.1016/S0034-4257(02)00096-2.
65. Boschetti, M.; Bocchi, S.; Brivio, P.A. Assessment of Pasture Production in the Italian Alps Using Spectrometric and Remote Sensing Information. *Agric Ecosyst Environ* **2007**, *118*, 267–272, doi:10.1016/j.agee.2006.05.024.

66. Ren, H.; Zhou, G. Determination of Green Aboveground Biomass in Desert Steppe Using Litter-Soil-Adjusted Vegetation Index. *Eur J Remote Sens* **2014**, *47*, 611–625, doi:10.5721/EuJRS20144734.
67. Shanmugapriya, P.; Rathika, S.; Ramesh, T.; Janaki, P. Applications of Remote Sensing in Agriculture - A Review. *Int J Curr Microbiol Appl Sci* **2019**, *8*, 2270–2283, doi:10.20546/ijcmas.2019.801.238.
68. Wang, G.; Liu, S.; Liu, T.; Fu, Z.; Yu, J.; Xue, B. Modelling Above-Ground Biomass Based on Vegetation Indexes: A Modified Approach for Biomass Estimation in Semi-Arid Grasslands. *Int J Remote Sens* **2019**, *40*, 3835–3854, doi:10.1080/01431161.2018.1553319.
69. WANG, F.; HUANG, J.; TANG, Y.; WANG, X. New Vegetation Index and Its Application in Estimating Leaf Area Index of Rice. *Rice Sci* **2007**, *14*, 195–203, doi:10.1016/S1672-6308(07)60027-4.
70. Baumgartner, D.; Kolassa, J. Power Considerations for Kolmogorov–Smirnov and Anderson–Darling Two-Sample Tests. *Commun Stat Simul Comput* **2023**, *52*, 3137–3145, doi:10.1080/03610918.2021.1928193.
71. Yıldız, M.B.; Di Nunno, F.; Đurin, B.; Pham, Q.B.; de Marinis, G.; Granata, F. A Combined Seasonal Mann–Kendall and Innovative Approach for the Trend Analysis of Streamflow Rate in Two Croatian Rivers. *Water (Basel)* **2024**, *16*, 1422, doi:10.3390/w16101422.
72. Shadmani, M.; Marofi, S.; Roknian, M. Trend Analysis in Reference Evapotranspiration Using Mann-Kendall and Spearman's Rho Tests in Arid Regions of Iran. *Water Resources Management* **2012**, *26*, 211–224, doi:10.1007/s11269-011-9913-z.
73. Hamed, K.H.; Ramachandra Rao, A. A Modified Mann-Kendall Trend Test for Autocorrelated Data. *J Hydrol (Amst)* **1998**, *204*, 182–196, doi:10.1016/S0022-1694(97)00125-X.
74. Yue, S.; Wang, C. The Mann-Kendall Test Modified by Effective Sample Size to Detect Trend in Serially Correlated Hydrological Series. *Water Resources Management* **2004**, *18*, 201–218, doi:10.1023/B:WARM.0000043140.61082.60.
75. Yue, S.; Pilon, P.; Phinney, B.; Cavadias, G. The Influence of Autocorrelation on the Ability to Detect Trend in Hydrological Series. *Hydrol Process* **2002**, *16*, 1807–1829, doi:10.1002/hyp.1095.
76. Serinaldi, F.; Kilsby, C.G. The Importance of Prewhitening in Change Point Analysis under Persistence. *Stochastic Environmental Research and Risk Assessment* **2016**, *30*, 763–777, doi:10.1007/s00477-015-1041-5.
77. Patakamuri, S.K.; Muthiah, K.; Sridhar, V. Long-Term Homogeneity, Trend, and Change-Point Analysis of Rainfall in the Arid District of Ananthapuramu, Andhra Pradesh State, India. *Water (Basel)* **2020**, *12*, 211, doi:10.3390/w12010211.
78. Buhairi, M.H. Al Analysis of Monthly, Seasonal and Annual Air Temperature Variability and Trends in Taiz City - Republic of Yemen. *J Environ Prot (Irvine, Calif)* **2010**, *01*, 401–409, doi:10.4236/jep.2010.14046.
79. da Silva, R.M.; Santos, C.A.G.; Moreira, M.; Corte-Real, J.; Silva, V.C.L.; Medeiros, I.C. Rainfall and River Flow Trends Using Mann–Kendall and Sen's Slope Estimator Statistical Tests in the Cobres River Basin. *Natural Hazards* **2015**, *77*, 1205–1221, doi:10.1007/s11069-015-1644-7.
80. Jiqin, H.; Gelata, F.T.; Chaka Gemeda, S. Application of MK Trend and Test of Sen's Slope Estimator to Measure Impact of Climate Change on the Adoption of Conservation Agriculture in Ethiopia. *Journal of Water and Climate Change* **2023**, *14*, 977–988, doi:10.2166/wcc.2023.508.
81. Gocic, M.; Trajkovic, S. Analysis of Changes in Meteorological Variables Using Mann-Kendall and Sen's Slope Estimator Statistical Tests in Serbia. *Glob Planet Change* **2013**, *100*, 172–182, doi:10.1016/j.gloplacha.2012.10.014.
82. Sen, P.K. Estimates of the Regression Coefficient Based on Kendall's Tau. *J Am Stat Assoc* **1968**, *63*, 1379–1389, doi:10.1080/01621459.1968.10480934.
83. Liu, Z.; Wang, H.; Li, N.; Zhu, J.; Pan, Z.; Qin, F. Spatial and Temporal Characteristics and Driving Forces of Vegetation Changes in the Huaihe River Basin from 2003 to 2018. *Sustainability* **2020**, *12*, 2198, doi:10.3390/su12062198.
84. Li, C.; Qi, J.; Yang, L.; Wang, S.; Yang, W.; Zhu, G.; Zou, S.; Zhang, F. Regional Vegetation Dynamics and Its Response to Climate Change—a Case Study in the Tao River Basin in Northwestern China. *Environmental Research Letters* **2014**, *9*, 125003, doi:10.1088/1748-9326/9/12/125003.
85. Khaliq, A.; Comba, L.; Biglia, A.; Ricauda Aimonino, D.; Chiaberge, M.; Gay, P. Comparison of Satellite and UAV-Based Multispectral Imagery for Vineyard Variability Assessment. *Remote Sens (Basel)* **2019**, *11*, 436, doi:10.3390/rs11040436.